Renewable Energy 257 (2026) 124754

Contents lists available at ScienceDirect

Renewable Energy

journal homepage: www.elsevier.com/locate/renene

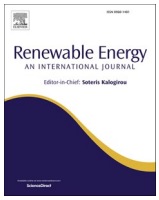

Enhanced power extraction in shaded photovoltaic arrays using dynamic reconfiguration with multi-objective nutcracker optimization algorithm

K. Eswaramoorthy [a,*], J. Viswanatha Rao [b], Viswaprakash Babu [c], P. Mukilan [d]

[a] Department of Electrical and Electronics Engineering, Saveetha Engineering College, Sriperumbadur, Chennai, 602105, Tamil Nadu, India
[b] Department of Electrical and Electronics Engineering, VNR Vignana Jyothi Institute of Engineering and Technology, Hyderabad, 500090, India
[c] Department of Electrical and Electronics Engineering, Kaveri University, Telangana, 502279, India
[d] Department of Electronics and Communication Engineering, Dhanalakshmi Srinivasan College of Engineering, Coimbatore, 641105, India

ARTICLE INFO

Keywords:
PV array reconfiguration
PSC
Multi-objective optimization
Mismatch reduction
MONOA

ABSTRACT

Photovoltaic (PV) array performance is notably affected by Partial Shading Conditions (PSCs) by causing mismatch losses, reducing energy output, and compromising system reliability. The proposed study outlines a dynamic reconfiguration strategy for PV arrays under PSC using the Multi-Objective Nutcracker Optimization Algorithm (MONOA). MONOA is a recently developed bio-inspired metaheuristic designed for multi-objective optimization problems. It integrates fast opposition-based learning, crowding distance and non-dominated sorting to effectively search for optimal PV switching configurations that maximize output power and minimize current imbalance and switching activity. A Total Cross-Tied (TCT) based 9 × 9 PV array is used as test system, and a novel Objective Function (OF) is proposed for enhancing solution quality without requiring weight tuning. The performance of MONOA is compared against well-established algorithms such as Improved Prairie Dog Optimization (IPDO), Atom Search Optimization (ASO), and African Vultures Optimization Algorithm (AVOA) under two different shading patterns. Simulation results demonstrate that MONOA consistently achieves higher power output, better fill factor, lower mismatch loss, and the fastest execution time among all tested methods.

1. Introduction

Studies conducted in recent years have prioritized enhancing maximal power harvesting from PV systems during fluctuating irradiation and temperature changes. Enhancing the power generation efficiency elevates the PV plant operational performance and reduces unit cost of generated power [1,2]. Solar PV is a preferred renewable source due to its abundant availability and year-round accessibility, even in remote and off-grid locations. Furthermore, it stands out for its affordable installation, convenient transportation and pollution-free operation [3,4]. Despite their efficiency, PV systems encounter electrical and physical problems, including shaded faults, converter switch faults, open circuit faults, line-to-line faults, hot spots and arc faults. At the same time, mismatch effects are a common issue in PV systems, leading to a drop in power generation efficiency due to module cracking or inconsistent radiation exposure across the array [5,6]. This effect, when present in PV arrays, results in significant power degradation, defined as discrepancy among the peak potential array power and aggregate maximum power of its modules [7]. When the radiation level varies across different sections of a PV array, despite consistent solar energy input per square meter, it leads to a condition known as partial shading. The shading conditions affecting PV systems are generally divided into static and dynamic types. The former is caused due to transient factors like clouds, leaves, dust and birds sitting on the panels, while the latter is caused by permanent features such as buildings and trees [8,9]. Fig. 1 clearly illustrates the PSC impact on Maximum Power Point (MPP).

In addition to performance degradation, PSC poses a threat to the integrity of PV system components, causing diode failures in the form of open or short circuits. Hence, when PSC affects a string, bypass diodes isolate underperforming modules by short-circuiting them [10]. To overcome MPPT challenges under partial shading, both passive and active solutions have been proposed. Passive methods, including bypass diodes and configurations like Series-Parallel (SP), Bridge-Link (BL), Honeycomb and Total-Cross-Tied (TCT) aim to reduce shading effects. Among these configurations, which are represented in Fig. 2, the TCT arrangement has demonstrated superior effectiveness in maximizing

* Corresponding author.
E-mail address: keswaramoorthy64@gmail.com (K. Eswaramoorthy).

https://doi.org/10.1016/j.renene.2025.124754
Received 9 June 2025; Received in revised form 17 September 2025; Accepted 8 November 2025
Available online 12 November 2025

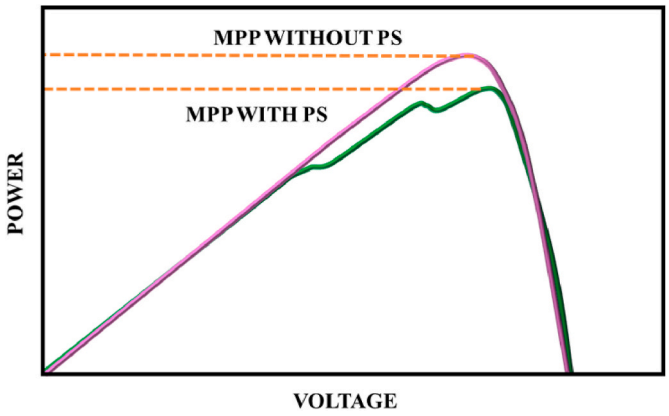

Fig. 1. MPP behaviour analysis in the presence of PSC.

output under PSCs [11].

Active techniques to mitigate PSC in PV systems are broadly categorized into three main approaches, where each offers distinct benefits and limitations. One method involves the use of multi-tracker converters, which allow different sections of the PV array to operate at their respective MPPs, thereby improving overall efficiency under uneven irradiance [12]. Another technique employs micro converters, where each panel or a small group of panels is equipped with its own power converter, enhancing granularity in control and power optimization. The third approach focuses on reconfiguring PV arrays to adapt to shading patterns, ensuring more uniform power generation and minimizing mismatch losses [13,14]. Generally, PV module reconfiguration techniques are divided into static and dynamic types. Dynamic approaches, including Electrical Array Reconfiguration (EAR), involve actively modifying the electrical configuration of modules to optimize performance under partial shading conditions. Static approaches maintain a constant electrical setup and involve only the physical rearrangement of modules [15]. Compared to static methods, dynamic approaches enhance the operational efficiency of PV systems, especially under PSCs. Unlike static techniques, which involve fixed physical rearrangement of modules, dynamic reconfiguration adjusts electrical connections in real time without altering the physical layout. This adaptability allows for optimal power extraction by minimizing mismatch losses and maintaining high efficiency as shading patterns change. Additionally, dynamic systems are easier to automate, require less maintenance, and eliminate the need for manual intervention, making them more suitable for large-scale and smart PV systems [16,17].

However, existing dynamic reconfiguration approaches for PV systems under partial shading conditions face certain limitations that affect

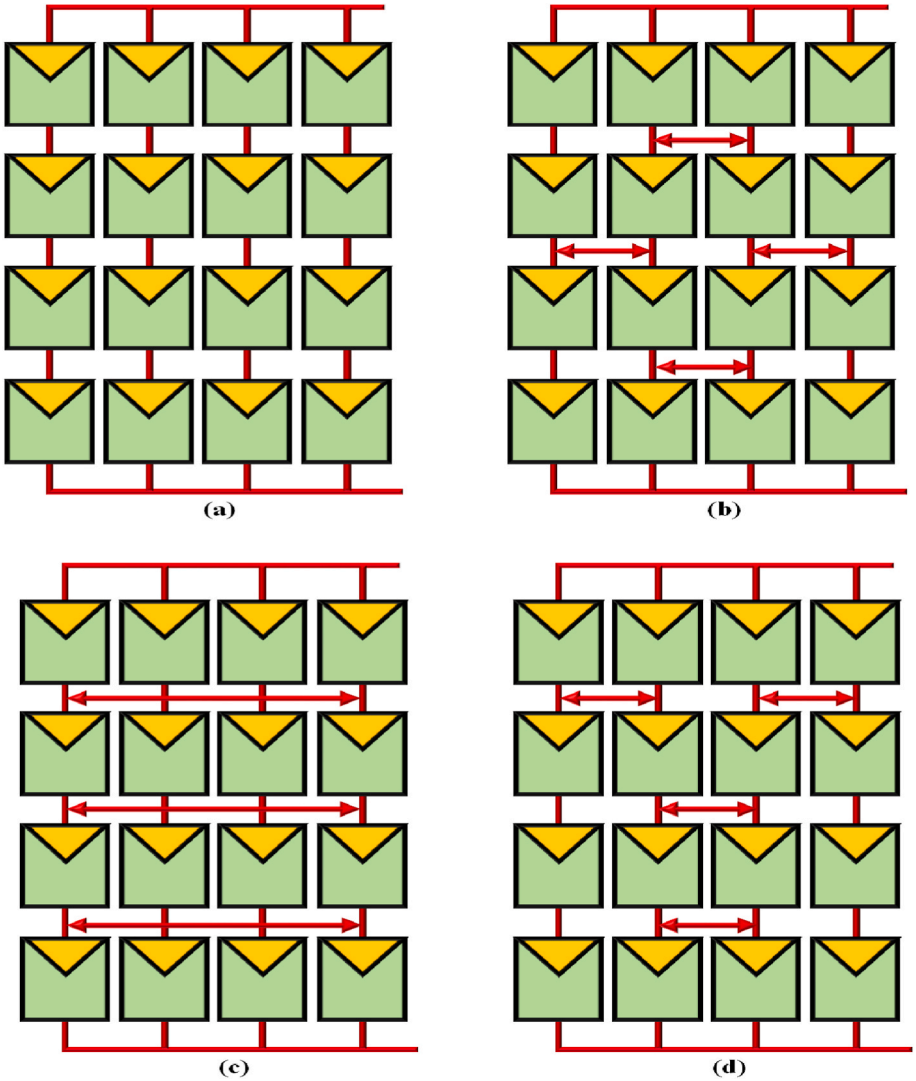

Fig. 2. Different PV module interconnection configurations (a) SP (b) BL (c) TCT and (d) Honeycomb.

their efficiency and practicality. Many methods rely on heuristic or single-objective optimization techniques, which often prioritize maximizing power extraction but neglect important aspects such as switching activity, execution time, or mismatch current reduction, leading to suboptimal long-term performance [18]. Some algorithms, such as traditional swarm-based or evolutionary approaches, suffer from slow convergence, high computational demand and susceptibility to local optima, which makes them less suitable for real-time implementation [19]. Moreover, several strategies require frequent and large-scale switching of array interconnections, resulting in increased hardware wear, higher control complexity, and added energy losses during transitions. Another major issue is the dependence on weight-based objective functions, where improper weight selection can bias the optimization and reduce robustness across different shading scenarios. Finally, scalability remains a challenge, as many existing methods struggle to maintain efficiency and low computational cost when applied to large-scale PV arrays, limiting their deployment in utility-level solar farms [20,21]. A summary of research works on dynamic reconfiguration of PV modules, along with their pros and cons, is provided in Table 1.

In this research. MONOA is implemented for the dynamic reconfiguration of PV array under PSC. This technique maximizes the power output, minimizes the number of switching actions in addition to reducing component wear and reconfiguration frequency. With the incorporation of multi-objective framework, MONOA offers a more holistic and practical solution. It also promotes long-term PV system efficiency and durability. The adaptive nature of the optimization algorithm enables better responsiveness to variable shading patterns.

2. System modelling

2.1. PV module modelling

Modelling of PV cell is imperative in its design process as it ultimately contributes to the heightened efficiency of the entire PV system. PV cells, when accurately modelled, effectively replicate the actual performance of a PV system. Nevertheless, the development of such model is difficult due to the inherent non-linearity of the cells. Consequently, significant efforts have been devoted by several researchers for developing an accurate PV model that enhances plant efficiency. These efforts involve comprehensive analysis and range of optimization techniques that has led to the evolution of primary diode-based PV models. Due to fewer parameters, simpler design and ease of implementation, the single-diode PV model is generally chosen over the other two models. Fig. 3 provides the PV model electric circuit diagram, encompassing a current source I_{PV}, which is coupled counter parallel to diode D_1. Here, KCL is used for evaluating the produced model current,

$$I = I_{PV} - I_{D_1} - I_P \tag{1}$$

In the above equation, I_{PV} specifies PV source current, I_{D_1} is diode current and I_P current across shunt resistance R_p. With the substitution of I_{D_1} and I_P in Equation (1),

$$I = I_{PV} - I_{01}\left(exp\left(\frac{V_{D_1}}{a_1 V_t} - 1\right)\right) - \left(\frac{V + IR_s}{R_p}\right) \tag{2}$$

In this equation, the thermal voltage is specified as V_t and is computed using the expression $\frac{N_s kT}{q}$, where the Boltzmann constant is specified as k. Moreover, the term I_{01} specifies diode leakage current, a_1 is the Ideality factor, N_s is count of series coupled cells and q is the electric charge of an electron. Given the strong influence of environmental condition on PV output, the generated current is mathematically defined as,

$$I_{PV} = \left(\frac{G}{G_0}\right)[I_{sc} + k_i(T - T_0)] \tag{3}$$

Table 1
Evaluation of dynamic PV reconfiguration strategies.

Ref	Technique	Strongpoints	Shortcomings
[22]	Fuzzy logic	Ensures rapid and accurate selection of optimal configurations, which are suitable for systems of various capacities.	Relying on short-circuit current for radiation estimation proves to be both complex and economically demanding.
[23]	Neuro-fuzzy algorithm	It is a fully automatic, online method that enhances PV array performance under PSC without requiring auxiliary modules.	Its reliance on global measurements limits detailed analysis of localized faults.
[24]	Improved Pelican Optimization algorithm	It simultaneously optimizes power output and minimizes switching actions.	The method optimizes one column at a time, which lead to local optima rather than a global best configuration.
[25]	Evolutionary based Pareto optimization algorithm	Minimizes the number of switch operations and comprises of multiple reconfiguration schemes.	Ineptness in handling fast-changing shading patterns.
[26]	Square Dynamic Reconfiguration (SDR)	This quadrant-based approach offers simple and structured design with low hardware complexity.	The fixed quadrant logic of this technique is its major shortcoming.
[27]	Genetic Algorithm (GA)	It provides improved power output and is capable of handling regular and irregular configurations.	The problem of premature convergence is its major limitation.
[28]	JAYA algorithm	It is a simple technique with low computational burden and improved power output.	It only considers power output and does not optimize switch count or system wear.
[29]	Improved Prairie Dog Optimization (IPDO)	The algorithm performs well on large arrays.	Cell-level switching is highly granular and demands a very complex switching matrix.
[30]	Atom Search Optimization (ASO)	This technique has fast execution time and significantly reduces mismatch losses.	It does not focus on minimizing switching actions.
[31]	African Vultures Optimization Algorithm (AVOA)	It offers high power enhancement with reduced power losses.	It does not minimize switching activity, component aging or reconfiguration frequency.

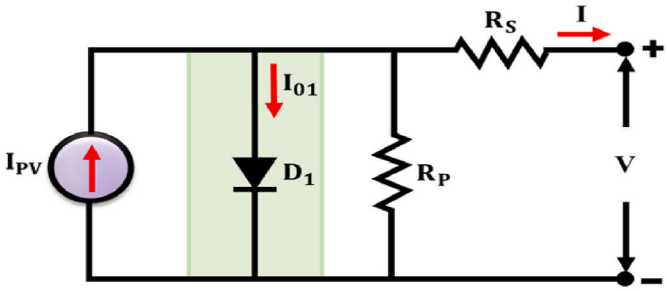

Fig. 3. Single diode electric circuit.

In this context, I_{sc} is the current measured when the terminals are shorted under standard test conditions (STC). Moreover, T and G are the actual temperature and irradiation values, respectively. Similarly, the value of $T_0 = 25°C$ and $G_0 = 1000W/m^2$. The current coefficient factor

is specified as k_i.

2.2. TCT topology for PV arrays

TCT is widely recognized as an effective connection strategy to meet power requirements. Research findings confirm its enhanced performance over BL, HC and SP connection methods. A TCT connection is created by linking each row of an SP layout using crossties. To demonstrate, a 9 × 9 TCT PV array is used, as seen in Fig. 4.

The configuration encompasses nine columns and nine rows. The voltage and current in a TCT-connected system are determined as,

$$V_{array} = \sum_{m=1}^{9} V_{M_m} \tag{4}$$

$$I_{R_m} = \sum_{n=1}^{9} \left(\frac{G_{mn}}{G_s} I_{M_{mn}} \right), m = 1, 2, 3, \ldots, 9 \tag{5}$$

In this equation, I_{R_m} is the generated current in row m, V_{array} is the total terminal voltage, while $I_{M_{mn}}$ and $V_{M_{mn}}$ correspond to module current and voltage in row x at STC $\left(G_s = 1000 \frac{W}{m^2} \right)$, respectively. To maximize the PV array power output, shading is required to be consistently and evenly distributed across the entire module surface. The TCT arrangement fails to achieve a uniform distribution under PSC. In addition, the TCT configuration demands a substantial switch count, calculated as $2 \times M \times (M+1) - 2 + 2 \times N \times (M \times N - M)$ with N and M indicating the total count of columns and rows in array.

Motivated by the need for simplicity and flexibility, a meta-heuristic optimization-based approach is proposed to identify the optimal switching matrix interconnection as shown in Fig. 5.

2.3. Formulation of objective function (OF)

Establishing OF is a fundamental requirement, in order to maximize power output under uniformly distributed shading, a novel OF is proposed. This function is defined as the ratio of the total power produced by the PV array to the absolute error between the maximum and minimum row currents, and is formulated as follows,

$$Maximize(obj(i)) = \frac{Array_{power}}{|I_{max} - I_{min}| + \in} \tag{6}$$

In this equation, the i-th element fitness value is represented as $obj(i)$, $\in$ is a positive constant preventing singularity without significantly altering the optimization process. This ensures numerical stability and avoids abrupt changes in the objective function when current imbalance is minimal. Additionally, under conditions where $I_{max} \approx I_{min}$, the system is already well-balanced with negligible mismatch losses, meaning that maximizing array power naturally dominates the optimization. In the row current vector $I = [I_1, I_2, I_3, \ldots, I_9]$, I_{min} and I_{max} indicate the lowest and highest current values, respectively. The total array output power is,

$$Array_{power} = \sum_{m=1}^{X} I_{R_m} \times V_m \tag{7}$$

The core objective is to enhance power output while reducing the difference between the highest and lowest row currents, thereby maintaining a uniform shading pattern on the PV surface.

2.4. Dynamic reconfiguration using MONOA

MONOA is a recently developed nature-inspired metaheuristic designed for multi-objective optimization problems, and it has been adapted here for PV array reconfiguration under PSC. It builds upon the Nutcracker Optimization Algorithm (NOA), a single-objective optimizer inspired by the foraging and caching behaviour of nutcracker birds. In NOA's metaphor, each candidate solution is a nutcracker bird, and the algorithmic operators mimic the bird's strategies for gathering seeds and storing them for future use. MONOA extends NOA by incorporating three key enhancements to handle multiple objectives: an opposite-learning strategy for initialization, a fast Non-Dominated Sorting (NDS) approach, and a crowding distance mechanism for Pareto-optimal selection. These additions ensure that MONOA evolves a diverse set of non-dominated solutions and converge toward the Pareto front of the multi-objective problem. In the context of PV reconfiguration, each nutcracker agent's position encodes a particular wiring configuration. The algorithm iteratively updates these positions through a series of exploration and exploitation phases named after the bird's behaviours: foraging, storage, cache-search and recovery, each governed by specific mathematical update rules. Through these phases, MONOA alternates between exploring new configurations and exploiting knowledge of the best-found configurations, all while evaluating solutions on multiple objectives and using Pareto-based criteria to guide the search toward an optimal reconfiguration. Fig. 6 indicates the flowchart of MONOA for dynamic reconfiguration of PV arrays. The algorithm starts with an opposition-based population initialization, where for each randomly initialized position $X_{i,j}(0)$, its opposite is generated as,

$$X_{ij}^{opp}(0) = L_j + U_j - X_{i,j}(0) \tag{8}$$

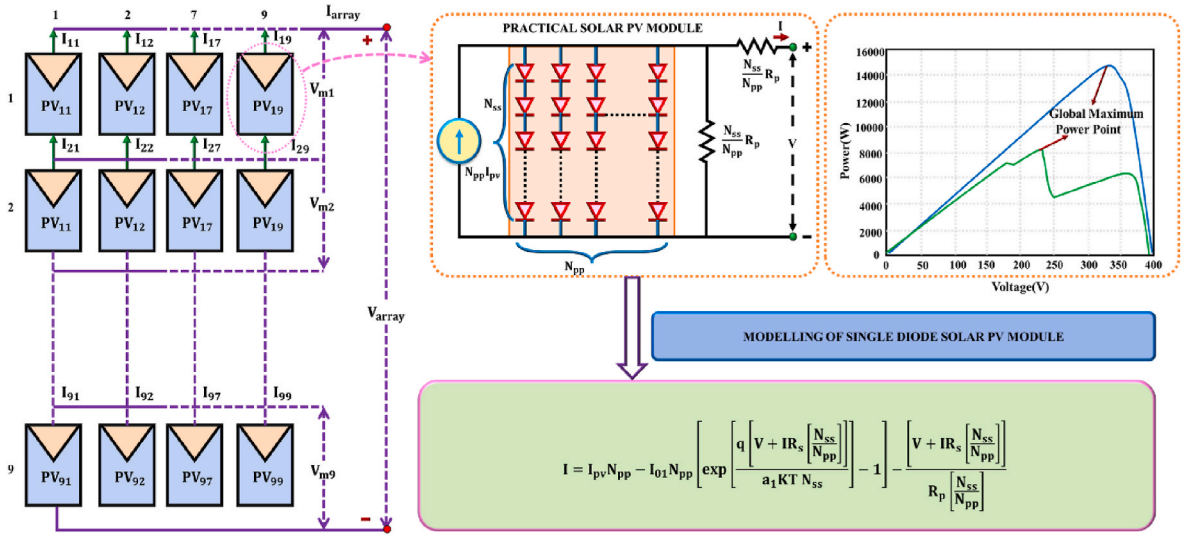

Fig. 4. PV module behaviour in a TCT-connected 9 × 9 solar array.

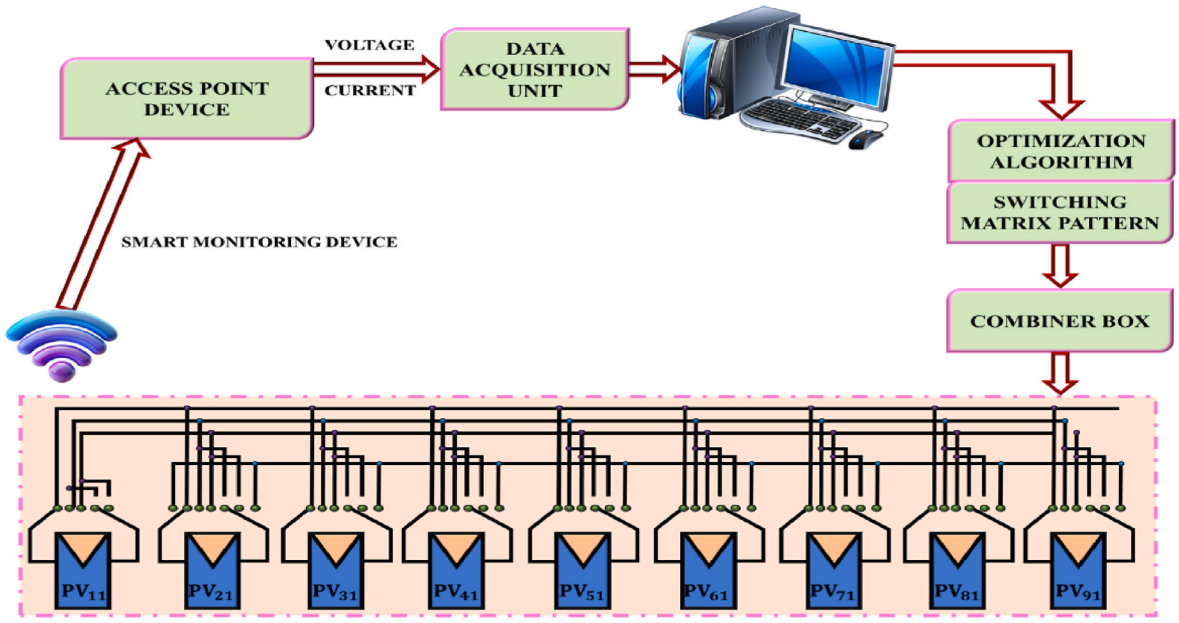

Fig. 5. Adaptive PV reconfiguration using switching patterns for optimal switching matrix interconnection.

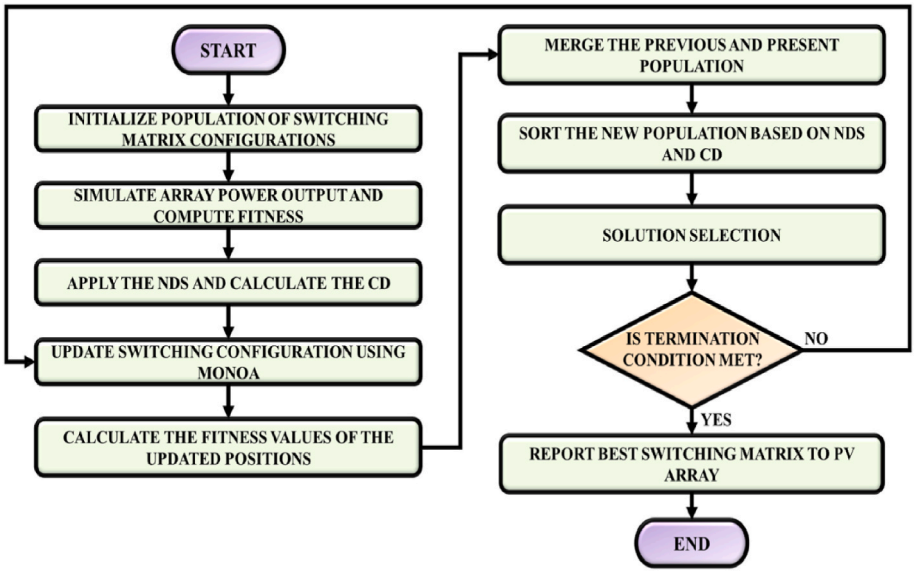

Fig. 6. Flowchart of MONOA for dynamic reconfiguration of PV arrays.

Where, L_j and U_j are the lower and upper bounds of the j-th dimension. During the foraging phase, an agent updates its position based on population mean and random influences as,

$$X_{i,j}^{t+1} = \begin{cases} X_{m,j}^{t} + \gamma\left(X_{A,j}^{t} - X_{B,j}^{t}\right) + \mu r_2\left(U_j - L_j\right), if\, \tau_1 < \tau_2 and t \le \dfrac{T_{max}}{2} \\ X_{C,j}^{t} + \mu\left(X_{A,j}^{t} - X_{B,j}^{t}\right)\mu \cdot 1(r_1 < \delta) \cdot r_2\left(U_j - L_j\right), if\, \tau_1 < \tau_2 and t > \dfrac{T_{max}}{2} \\ X_{i,j}^{t}, otherwise \end{cases} \tag{9}$$

Where, X_A, X_B, X_C are randomly selected agents, X_m is the mean position, γ is a Lévy-distributed step and μ is the switching coefficient selected as,

$$\mu = \begin{cases} \tau_3, r_1 < r_2 \\ \tau_4, r_2 < r_3 \\ \tau_5, otherwise \end{cases} \tag{10}$$

With τ_3, τ_4, τ_5 as random values drawn from predefined distributions. The storage phase moves the solution towards the best found so far,

$$X_{i,j}^{t+1} = X_i^t + l \cdot \gamma' \cdot \left(X_{best}^t - X_i^t\right) \tag{11}$$

Where, $l = 1 - \frac{t}{T_{max}}$ linearly decreases over time and γ' is a Lévy step. In the cache-search phase, the agent generates two reference points, RP1 and RP2. If $\theta = \frac{\pi}{2}$, RP1 is calculated as,

$$RP1_i^t = X_i^t + \alpha \cos(\theta)\left(X_A^t - X_B^t\right) + \alpha RP \tag{12}$$

and otherwise as,

$$RP1_i^t = X_i^t + \alpha\left(X_A^t - X_B^t\right) + \alpha RP \tag{13}$$

RP2 is similarly generated using,

$$RP2_i^t = X_i^t + \alpha(U - L) \tag{14}$$

The convergence control parameter α is defined as,

$$\alpha = \begin{cases} \left(1 - \frac{t}{T_{max}}\right)^{\lambda}, r_1 > r_2 \\ \left(\frac{t}{T_{max}}\right)^{\lambda}, otherwise \end{cases} \tag{15}$$

The agent then updates its position toward RP1 using,

$$X_i^{t+1} = X_i^t + \chi\left(RP1_i^t - X_i^t\right) \tag{16}$$

If the solution does not improve, the agent performs the recovery phase, where the position is updated using RP2 and the best-known solution,

$$X_{i,j}^{t+1} = X_{best,j}^t + \rho_1\left(RP_j - X_{best,j}^t\right) + \rho_2\left(C_j^t - RP_j\right) \tag{17}$$

Alternatively,

$$X_i^{t+1} = X_i^t + \chi'\left(RP2_i^t - X_i^t\right) \tag{18}$$

MONOA also employs fast non-dominated sorting to classify solutions based on Pareto dominance, and crowding distance to maintain solution diversity,

$$CD_i = \sum_{j=1}^{M} \frac{f_j(i+1) - f_j(i-1)}{f_j^{max} - f_j^{min}} \tag{19}$$

Where, f_j is the j-th objective and M is the number of objectives.

Table 2 lists out the parameters of MONOA which are tuned using Cross-validation. This involves systematically testing different parameter settings across multiple partial shading scenarios to identify values that deliver consistently good performance rather than optimizing for a single case. In practice, the dataset of shading patterns is divided into training and validation subsets: the training set is used to run MONOA with various combinations of population size, iteration limits and control parameters, while the validation set evaluates how well these tuned settings generalize to unseen conditions. Performance metrics such as obtained power, mismatch loss, fill factor and execution time are compared across folds and the parameter set that yields stable results with minimal variance is selected. This approach prevents overfitting of parameters to specific shading patterns and promotes that MONOA remains robust across a wide range of real-world operating conditions. Moreover, cross-validation provides insights into parameter sensitivity, helping designers strike a balance between computational efficiency and optimization accuracy, which is especially critical for real-time PV array reconfiguration.

The algorithm selects solutions with lower ranks and higher crowding distances. By iteratively applying these exploration and exploitation mechanisms, MONOA identifies an optimal or near-optimal set of PV module interconnections that maximize output power while minimizing current imbalance and switch usage. This strategy promotes robust PV performance in dynamically shaded environments with minimal loss and high adaptability.

Table 2
Parameters of MONOA.

Parameters	Values
Population size	50
Maximum iterations	100
Learning coefficient	0.5-1.0
Influence factor	0.1-0.9
Threshold probability	[0,1]

3. Results and discussion

In the first phase, the proposed MONOA is evaluated and compared with three contemporary optimization techniques: IPDO, AVOA and ASO. All three algorithms are implemented using the multi-objective fitness function designed for PV array reconfiguration under PSCs. This function aims to enhance the total power output of the array while minimizing current deviations across the rows. The goal of this comparison is to assess the effectiveness of MONOA in optimizing the switching configuration of the PV array and maintaining current uniformity, which is essential for mitigating mismatch losses. The second phase involves a comprehensive performance analysis using multiple evaluation metrics. These metrics help determine the consistency, efficiency, and robustness of MONOA when compared to IPDO, AVOA and ASO across different shading scenarios. The simulations are conducted on a 9×9 PV array configured in a TCT topology. Each algorithm is executed for 30 independent runs, with a population size of 20 and 100 iterations per run. The simulation environment is set up on MATLAB. The electrical parameters of the PV module are: Short-Circuit Current = 5.2 A and Open-Circuit Voltage = 44.2 V.

To analyse the effectiveness of the proposed OF, this section presents a comparative evaluation of algorithm performance using both the conventional weighted OF and the newly formulated one. The analysis is conducted using a 9×9 PV array subjected to two types of PSCs, which are the short broad (pattern 1) and long broad (pattern 2) shading,

- Pattern 1 involves different sunlight levels across the array: 900, 800, 600, 400, and 200 W/m^2.
- Pattern 2 has the first six columns fully illuminated (900 W/m^2), while the others receive reduced irradiance of 800, 700, 400, and 300 W/m^2.

Fig. 7 (a) and 7 (b) and 8 (a), 8 (b) show the TCT-connected shaded PV array and the reconfigured layouts generated depending on both the traditional weighted objective function and the proposed one, for pattern 1 and pattern 2, respectively. The related values of current, voltage, and power are calculated and listed in Tables 3–6 for each pattern (appendix). The methodology used to compute the row-wise current, voltage, and power for pattern 1, as shown in Figs. 7 and 8, is detailed in the appendix section.

Figs. 9 and 10 illustrate the I–V and P–V characteristics of the proposed MONOA algorithm in comparison with IPDO, AVOA, ASO and the traditional TCT configuration under shading patterns 1 and 2. In both cases, the TCT method demonstrates significantly lower performance, with multiple power peaks, sharp drops in current and clear mismatch losses due to partial shading. In contrast, MONOA consistently delivers the highest and most stable power output, indicating effective PV array reconfiguration and strong mitigation of current mismatches.

Table 7 presents the performance of various PV array reconfiguration algorithms in terms of power extraction and mismatch loss under two partial shading patterns. For both patterns, the traditional TCT configuration shows the lowest obtained power output and the highest mismatch loss, confirming its limited ability to handle mismatch effects. Among the metaheuristic algorithms, MONOA consistently demonstrates superior performance.

Table 8 presents the fill factor values for five PV reconfiguration methods under shading patterns 1 and 2. The results show that the traditional TCT method yields the lowest fill factor in both scenarios, with values of 0.495 and 0.681 for patterns 1 and 2, respectively; indicating poor efficiency and high mismatch losses. In contrast, all metaheuristic-based methods demonstrate significantly improved fill factors, reflecting enhanced power extraction and better utilization of the PV array. Among the algorithms, MONOA consistently achieves the highest fill factors.

Table 9 presents the mean execution times of various optimization algorithms used for PV array reconfiguration under shading patterns 1

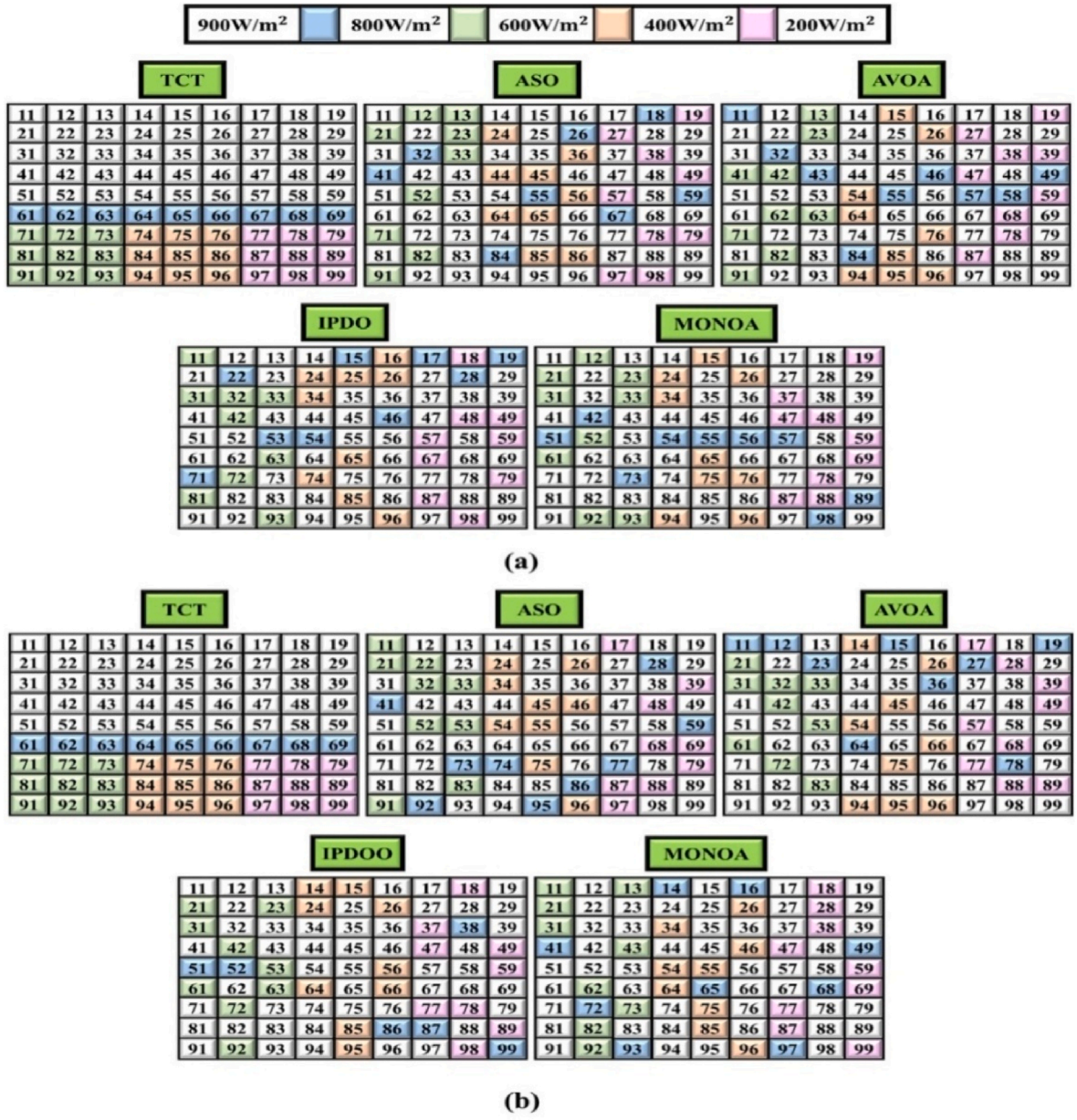

Fig. 7. Shading pattern distribution in PV array configurations optimized by different algorithms under pattern 1(a) Weighted OF and (b) proposed OF.

and 2. The results indicate that MONOA is the most computationally efficient approach, recording the lowest execution times of 0.3 s for pattern 1 and 0.32 s for pattern 2.

Table 10 summarizes the performance of the proposed MONOA algorithm under different operating conditions ranging from no shading to severe partial shading. In the absence of shading, MONOA is able to extract the full global peak of 14,617.349 W with zero mismatch loss, a high fill factor of 0.85 and the fastest execution time of 0.28 s, confirming its ability to fully utilize array capacity under ideal conditions. Under mild shading, the obtained power drops slightly to 13,137.476 W with a mismatch loss of 1479.873 W, while maintaining a high fill factor of 0.83 and similar execution time of 0.29 s. In the moderate shading scenario, power extraction reduces further to 11,657.603 W with a mismatch loss of 2959.746 W and a fill factor of 0.812, highlighting the growing effect of mismatch losses; execution time remains within 0.32 s, showing the algorithm's consistency in convergence speed. Under severe shading, MONOA still delivers 10,521.470 W while limiting mismatch loss to 4095.879 W and maintaining a reasonable fill factor of 0.792, again with a rapid convergence time of 0.32 s.

Table 11 presents the comparison of switching activity across different PV array reconfiguration approaches. The results indicate that traditional metaheuristic methods such as ASO and AVOA involve relatively high switching activity, requiring 40 and 36 switch operations per reconfiguration, respectively, which scale up to 240 and 216 switches per hour if six reconfigurations occur per hour. MOPSO and NSGA-II show moderate switching requirements, averaging 30 and 26 operations per reconfiguration, corresponding to 180 and 156 per hour. IPDO further reduces the switching activity to 22 per reconfiguration, reflecting better efficiency in minimizing unnecessary rewirings. In contrast, the proposed MONOA achieves the lowest switching activity, requiring only 10 switches per reconfiguration, which corresponds to 60 switches per hour representing a significant reduction of approximately 75 % compared to ASO. This reduction highlights MONOA's capability to balance power extraction with minimal switching overhead, leading to lower hardware stress, extended switch lifespan, and improved system reliability.

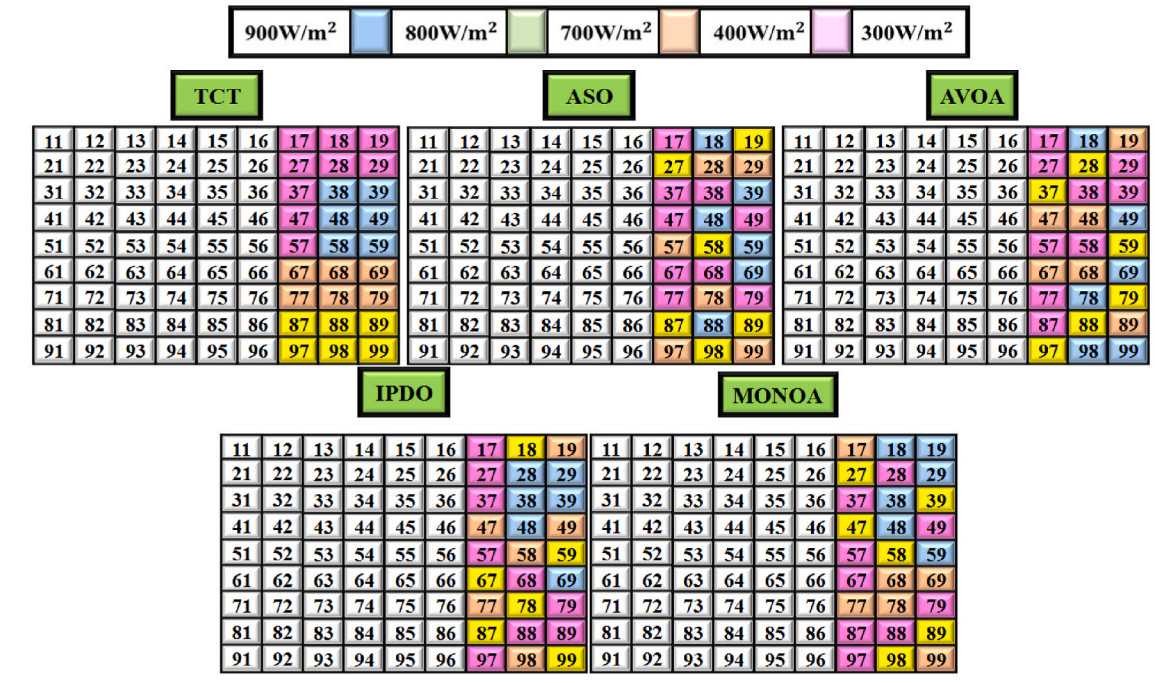

Fig. 8. Shading pattern distribution in PV array configurations optimized by different algorithms under pattern 2 (a) Weighted OF and (b) proposed OF.

3.1. Real-time applicability of the concept

For real-time implementation of the proposed MONOA-based dynamic reconfiguration strategy, several prerequisites and considerations must be addressed to ensure practical applicability. First, fast and reliable measurement of PV array parameters such as voltage, current and irradiance is essential, requiring accurate sensors and efficient data acquisition systems. The algorithm itself must exhibit low computational complexity and rapid convergence, as real-time reconfiguration demands decisions within milliseconds to seconds to track fast-changing shading patterns. Hardware platforms should be capable of supporting parallel processing and handling the switching operations without introducing delays or excessive energy overhead. Furthermore, robustness against measurement noise, communication delays and hardware switching constraints must be ensured to maintain stability and accuracy. System-level considerations, including scalability for

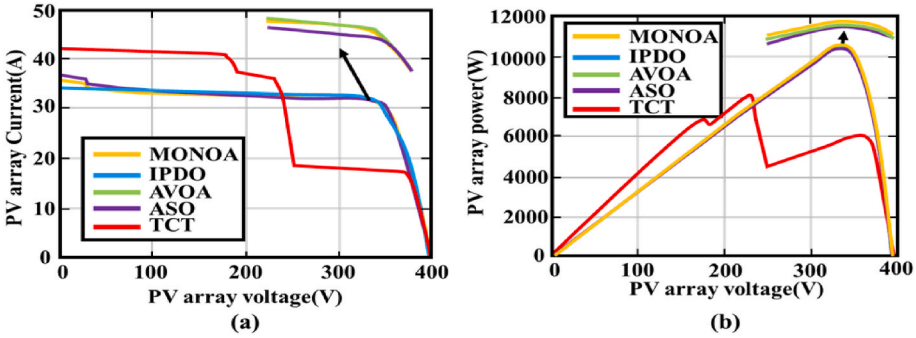

Fig. 9. Performance comparison assessment in pattern 1 for algorithms using I-V and P-V characteristics.

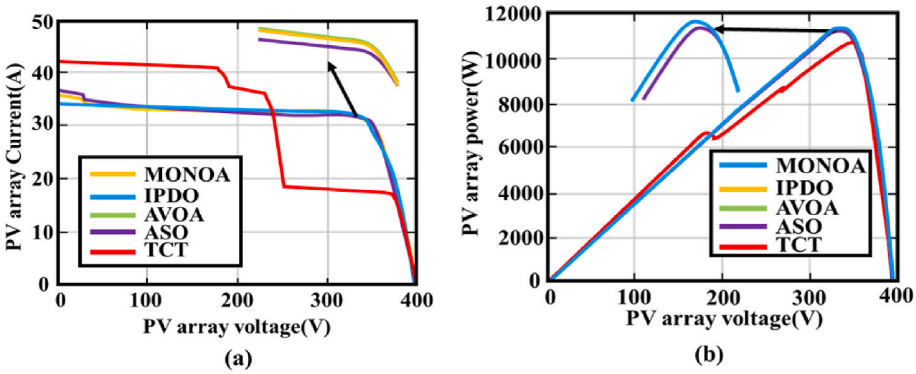

Fig. 10. Performance comparison assessment in pattern 2 for algorithms using I-V and P-V characteristics.

Table 7
Performance analysis of PV reconfiguration methods based on power extraction and mismatch loss.

Approach	Pattern 1			Pattern 2		
	Real GP (W)	Obtained GP (W)	Mismatch Loss (W)	Real GP (W)	Obtained GP (W)	Mismatch Loss (W)
TCT	14617.349	8168.949	6448.400	14617.349	10798.578	3818.771
ASO	14617.349	10417.625	4199.724	14617.349	11503.609	3113.740
AVOA	14617.349	10521.470	4095.879	14617.349	11549.155	3068.194
IPDO	14617.349	10484.241	4133.108	14617.349	11556.603	3060.746
MOPSO	14617.349	10500.000	4117.349	14617.349	11600.000	3017.349
NSGA-II	14617.349	10510.000	4107.349	14617.349	11620.000	2959.349
MONOA	14617.349	10521.470	4095.879	14617.349	11657.603	2959.746

Table 8
Performance analysis of PV reconfiguration methods based on Fill factor.

AVOA	0.782	0.778
IPDO	0.750	0.787
MOPSO	0.785	0.795
NSGA-II	0.789	0.801
MONOA	0.792	0.812

Table 9
Performance analysis of PV reconfiguration methods based on mean execution time.

Approach	Pattern 1	Pattern 2
ASO	1.2s	1.18s
AVOA	1.11s	1.14s
IPDO	0.42s	0.43s
MOPSO	0.65s	0.67s
NSGA-II	0.72s	0.74s
MONOA	0.3s	0.32s

Table 10
Performance analysis of MONOA under varying conditions.

Conditions	Real GP (W)	Obtained GP (W)	Mismatch loss (W)	Fill factor	Execution time (s)
No shading	14,617.349	14,617.349	0.000	0.850	0.28
Mild shading	14,617.349	13,137.476	1479.873	0.830	0.29
Moderate shading	14,617.349	11,657.603	2,9559.746	0.812	0.32
Severe shading	14,617.349	10,521.470	4095.879	0.792	0.32

large PV arrays, minimization of switching frequency to avoid wear on relays or power electronics and integration with existing MPPT units, are also critical. Overall, achieving real-time applicability requires balancing computational efficiency, hardware compatibility and operational reliability to ensure the algorithm transitions effectively from simulation to field deployment.

The proposed MONOA-based reconfiguration concept shows strong potential for managing larger PV arrays, as its multi-objective framework efficiently balances power extraction, mismatch loss reduction and

Table 11
Comparison of switching activity for reconfiguration approaches.

Approaches	Average switches/reconfiguration	Estimated switches/hour
ASO	40	240
AVOA	36	216
IPDO	22	132
MOPSO	30	180
NSGA-II	26	156
MONOA	10	60

computational speed. Unlike conventional methods such as TCT, which scale poorly with array size due to fixed interconnections, MONOA integrates adaptive mechanisms to handle the exponentially increasing configuration possibilities in larger arrays. Its fast execution time, demonstrated in smaller arrays, suggests scalability when extended to larger systems, provided that computational resources are proportionally allocated. Moreover, parallelization of MONOA's operations further enhances its capability to process high-dimensional search spaces. This ensures that even with hundreds or thousands of PV modules, the algorithm dynamically reconfigures arrays in near real-time, making it well-suited for utility-scale solar farms under diverse shading and fault conditions.

4. Conclusion

This study presents a dynamic PV array reconfiguration approach utilizing MONOA to mitigate the impact of partial shading conditions. By integrating a novel objective function that eliminates the need for weight tuning, the proposed method enhances both the power output and current uniformity across the PV array. Simulation results on a 9×9 TCT-configured array demonstrate the superiority of MONOA compared to other optimization techniques such as IPDO, ASO and AVOA. MONOA consistently achieves the highest obtained power, lowest mismatch loss, and best fill factor under both shading patterns tested. Moreover, it demonstrates the shortest execution time, indicating its potential for real-time applications. The enhanced performance is attributed to MONOA's balanced exploration-exploitation strategy and its ability to maintain diversity through crowding distance and Pareto-based selection. The overall findings confirm that MONOA is not only computationally efficient but also highly effective in maximizing energy harvesting in dynamically shaded PV systems. Therefore, it stands as a promising candidate for smart reconfiguration in large-scale solar installations, where adaptability and optimization efficiency are critical for sustained energy output.

CRediT authorship contribution statement

K. Eswaramoorthy: Writing – original draft, Data curation, Conceptualization. **J. Viswanatha Rao:** Writing – review & editing, Validation, Supervision, Project administration. **Viswaprakash Babu:** Writing – review & editing, Validation, Supervision, Project administration. **P. Mukilan:** Writing – review & editing, Validation, Supervision, Project administration.

Ethics approval

Not applicable.

Availability of data and materials

Data sharing is not applicable.

Funding

The authors received no specific funding for this study.

Declaration of competing interest

The authors declare that they have no known competing financial interests or personal relationships that could have appeared to influence the work reported in this paper.

Appendix

As per the TCT structure, the calculation of row currents is as follows. The first five rows exhibit identical current values, all obtained through the same computation,

$$I_{R1}toI_{R5} = 9\left(\frac{900}{1000}\right)I_M = 8.1I_M \tag{20}$$

The sixth-row's row currents are computed as,

$$I_{R6} = 9\left(\frac{800}{1000}\right)I_M = 7.2I_M \tag{21}$$

The seventh, eighth and ninth row's row currents are computed as,

$$I_{R7} = I_{R8} = I_{R9} = 3\left(\frac{600}{1000}\right)I_M + 3\left(\frac{400}{1000}\right)I_M + 3\left(\frac{200}{1000}\right)I_M = 3.6I_M \tag{22}$$

Using the weighted OF depicted in Fig. 8 (a), ASO algorithm evaluates row currents as follows,
For first row,

$$I_{R1} = 5\left(\frac{900}{1000}\right)I_M + 1\left(\frac{800}{1000}\right)I_M + 2\left(\frac{600}{1000}\right)I_M + 1\left(\frac{200}{1000}\right)I_M = 6.7I_M \tag{23}$$

For second row,

$$I_{R2} = 4\left(\frac{900}{1000}\right)I_M + 1\left(\frac{800}{1000}\right)I_M + 2\left(\frac{600}{1000}\right)I_M + 1\left(\frac{400}{1000}\right)I_M + 1\left(\frac{200}{1000}\right)I_M = 6.2I_M \tag{24}$$

For third row,

$$I_{R3} = 5\left(\frac{900}{1000}\right)I_M + 1\left(\frac{800}{1000}\right)I_M + 1\left(\frac{600}{1000}\right)I_M + 1\left(\frac{400}{1000}\right)I_M + 1\left(\frac{200}{1000}\right)I_M = 6.5I_M \tag{25}$$

For fourth row,

$$I_{R4}=5\left(\frac{900}{1000}\right)I_M+1\left(\frac{800}{1000}\right)I_M+2\left(\frac{400}{1000}\right)I_M+1\left(\frac{200}{1000}\right)I_M=6.3I_M \tag{26}$$

For fifth row,

$$I_{R5}=4\left(\frac{900}{1000}\right)I_M+2\left(\frac{800}{1000}\right)I_M+1\left(\frac{600}{1000}\right)I_M+1\left(\frac{400}{1000}\right)I_M+1\left(\frac{200}{1000}\right)I_M=6.4I_M \tag{27}$$

For sixth row,

$$I_{R6}=5\left(\frac{900}{1000}\right)I_M+2\left(\frac{800}{1000}\right)I_M+2\left(\frac{400}{1000}\right)I_M=6.9I_M \tag{28}$$

For seventh row,

$$I_{R7}=6\left(\frac{900}{1000}\right)I_M+1\left(\frac{600}{1000}\right)I_M+2\left(\frac{200}{1000}\right)I_M=6.4I_M \tag{29}$$

For eighth row,

$$I_{R8}=5\left(\frac{900}{1000}\right)I_M+1\left(\frac{800}{1000}\right)I_M+1\left(\frac{600}{1000}\right)I_M+2\left(\frac{400}{1000}\right)I_M=6.7I_M \tag{30}$$

For ninth row,

$$I_{R9}=6\left(\frac{900}{1000}\right)I_M+1\left(\frac{600}{1000}\right)I_M+2\left(\frac{200}{1000}\right)I_M=6.4I_M \tag{31}$$

Using the novel OF depicted in Fig. 8 (b), ASO algorithm evaluates row currents as follows, For first row,

$$I_{R1}=7\left(\frac{900}{1000}\right)I_M+1\left(\frac{600}{1000}\right)I_M+1\left(\frac{200}{1000}\right)I_M=7.1I_M \tag{32}$$

For second row,

$$I_{R2}=4\left(\frac{900}{1000}\right)I_M+1\left(\frac{800}{1000}\right)I_M+2\left(\frac{600}{1000}\right)I_M+2\left(\frac{400}{1000}\right)I_M=6.4I_M \tag{33}$$

For third row,

$$I_{R3}=5\left(\frac{900}{1000}\right)I_M+2\left(\frac{600}{1000}\right)I_M+1\left(\frac{400}{1000}\right)I_M+1\left(\frac{200}{1000}\right)I_M=6.3I_M \tag{34}$$

For fourth row,

$$I_{R4}=4\left(\frac{900}{1000}\right)I_M+1\left(\frac{800}{1000}\right)I_M+2\left(\frac{600}{1000}\right)I_M+2\left(\frac{400}{1000}\right)I_M+1\left(\frac{200}{1000}\right)I_M=6.3I_M \tag{35}$$

For fifth row,

$$I_{R5}=4\left(\frac{900}{1000}\right)I_M+1\left(\frac{800}{1000}\right)I_M+2\left(\frac{600}{1000}\right)I_M+2\left(\frac{400}{1000}\right)I_M=6.4I_M \tag{36}$$

For sixth row,

$$I_{R6}=7\left(\frac{900}{1000}\right)I_M+2\left(\frac{200}{1000}\right)I_M=6.7I_M \tag{37}$$

Table III
Row currents and power output analysis for various reconfiguration algorithms using weighted OF for pattern 1

TCT				ASO			
I_{R_i}	$V_m(V)$	$I_R(A)$	$P(W)$	I_{R_i}	$V_m(V)$	$I_R(A)$	$P(W)$
I_{R_1}	5 V_M	8.1 I_M	40.5 V_MI_M	I_{R_2}	9 V_M	6.2 I_M	55.8 V_MI_M
I_{R_2}	5 V_M	8.1 I_M	40.5 V_MI_M	I_{R_4}	8 V_M	6.3 I_M	50.4 V_MI_M
I_{R_3}	5 V_M	8.1 I_M	40.5 V_MI_M	I_{R_5}	7 V_M	6.4 I_M	44.8 V_MI_M
I_{R_4}	5 V_M	8.1 I_M	40.5 V_MI_M	I_{R_7}	7 V_M	6.4 I_M	44.8 V_MI_M
I_{R_5}	5 V_M	8.1 I_M	40.5 V_MI_M	I_{R_9}	7 V_M	6.4 I_M	44.8 V_MI_M
I_{R_6}	6 V_M	7.2 I_M	43.2 V_MI_M	I_{R_3}	4 V_M	6.5 I_M	26 V_MI_M
I_{R_7}	9 V_M	3.6 I_M	32.4 V_MI_M	I_{R_1}	3 V_M	6.7 I_M	20.1 V_MI_M
I_{R_8}	9 V_M	3.6 I_M	32.4 V_MI_M	I_{R_8}	3 V_M	6.7 I_M	20.1 V_MI_M

(*continued on next page*)

Table III (*continued*)

TCT				ASO			
I_{R_i}	$V_m(V)$	$I_R(A)$	$P(W)$	I_{R_i}	$V_m(V)$	$I_R(A)$	$P(W)$
I_{R_9}	9 V_M	3.6 I_M	32.4 $V_M I_M$	I_{R_6}	1 V_M	6.9 I_M	6.9 $V_M I_M$
AVOA				IPDO			
I_{R_i}	$V_m(V)$	$I_R(A)$	$P(W)$	I_{R_i}	$V_m(V)$	$I_R(A)$	$P(W)$
I_{R_6}	9 V_M	6.3 I_M	56.7 $V_M I_M$	I_{R_1}	9 V_M	6.3 I_M	56.7 $V_M I_M$
I_{R_9}	9 V_M	6.3 I_M	56.7 $V_M I_M$	I_{R_4}	9 V_M	6.3 I_M	56.7 $V_M I_M$
I_{R_1}	7 V_M	6.5 I_M	45.5 $V_M I_M$	I_{R_2}	7V_M	6.4 I_M	44.8 $V_M I_M$
I_{R_4}	7 V_M	6.5 I_M	45.5 $V_M I_M$	I_{R_5}	6V_M	6.5 I_M	39 $V_M I_M$
I_{R_8}	7 V_M	6.5 I_M	45.5 $V_M I_M$	I_{R_7}	6 V_M	6.5 I_M	26.4 $V_M I_M$
I_{R_2}	4 V_M	6.6 I_M	26.4 $V_M I_M$	I_{R_6}	4 V_M	6.6 I_M	26.4 $V_M I_M$
I_{R_3}	4 V_M	6.6 I_M	26.4 $V_M I_M$	I_{R_8}	4 V_M	6.6 I_M	26.4 $V_M I_M$
I_{R_5}	4 V_M	6.6 I_M	26.4 $V_M I_M$	I_{R_9}	4 V_M	6.6 I_M	26.4 $V_M I_M$
I_{R_7}	4 V_M	6.6 I_M	26.4 $V_M I_M$	I_{R_3}	1 V_M	6.7 I_M	6.7 $V_M I_M$
MONOA							
I_{R_i}		$V_m(V)$		$I_R(A)$			$P(W)$
I_{R_3}		9 V_M		6.3 I_M			56.7 $V_M I_M$
I_{R_7}		9 V_M		6.3 I_M			56.7 $V_M I_M$
I_{R_9}		7 V_M		6.4 I_M			44.8 $V_M I_M$
I_{R_2}		6 V_M		6.5 I_M			39 $V_M I_M$
I_{R_1}		5 V_M		6.6 I_M			33 $V_M I_M$
I_{R_4}		5 V_M		6.6 I_M			33 $V_M I_M$
I_{R_5}		5 V_M		6.6 I_M			33 $V_M I_M$
I_{R_6}		5 V_M		6.6 I_M			33 $V_M I_M$
I_{R_8}		5 V_M		6.6 I_M			33 $V_M I_M$

Table IV
Row currents and power output analysis for various reconfiguration algorithms using proposed OF for pattern 1

TCT				ASO			
I_{R_i}	$V_m(V)$	$I_R(A)$	$P(W)$	I_{R_i}	$V_m(V)$	$I_R(A)$	$P(W)$
I_{R_7}	9 V_M	3.6 I_M	$V_M I_M$	I_{R_3}	9 V_M	6.3 I_M	56.7 $V_M I_M$
I_{R_8}	9 V_M	3.6 I_M	$V_M I_M$	I_{R_4}	9 V_M	6.3 I_M	56.7 $V_M I_M$
I_{R_9}	9 V_M	3.6 I_M	$V_M I_M$	I_{R_8}	9 V_M	6.3 I_M	56.7 $V_M I_M$
I_{R_6}	6 V_M	7.2 I_M	$V_M I_M$	I_{R_2}	6 V_M	6.4 I_M	38.4 $V_M I_M$
I_{R_1}	5 V_M	8.1 I_M	$V_M I_M$	I_{R_5}	6 V_M	6.4 I_M	38.4 $V_M I_M$
I_{R_2}	5 V_M	8.1 I_M	$V_M I_M$	I_{R_9}	6 V_M	6.4 I_M	38.4 $V_M I_M$
I_{R_3}	5 V_M	8.1 I_M	$V_M I_M$	I_{R_7}	3 V_M	6.6 I_M	19.8 $V_M I_M$
I_{R_4}	5 V_M	8.1 I_M	$V_M I_M$	I_{R_6}	2 V_M	6.7 I_M	13.4 $V_M I_M$
I_{R_5}	5 V_M	8.1 I_M	$V_M I_M$	I_{R_1}	1 V_M	7.1 I_M	7.1 $V_M I_M$
AVOA				IPDO			
I_{R_i}	$V_m(V)$	$I_R(A)$	$P(W)$	I_{R_i}	$V_m(V)$	$I_R(A)$	$P(W)$
I_{R_2}	9 V_M	6.4 I_M	57.6 $V_M I_M$	I_{R_1}	9 V_M	6.4 I_M	57.6 $V_M I_M$
I_{R_3}	9 V_M	6.4 I_M	57.6 $V_M I_M$	I_{R_4}	9 V_M	6.4 I_M	57.6 $V_M I_M$
I_{R_8}	9 V_M	6.4 I_M	57.6 $V_M I_M$	I_{R_5}	9 V_M	6.4 I_M	57.6 $V_M I_M$
I_{R_1}	6 V_M	6.5 I_M	39 $V_M I_M$	I_{R_6}	9V_M	6.4 I_M	57.6 $V_M I_M$
I_{R_6}	6 V_M	6.5 I_M	39 $V_M I_M$	I_{R_7}	9V_M	6.4 I_M	57.6 $V_M I_M$
I_{R_7}	6 V_M	6.5 I_M	39 $V_M I_M$	I_{R_2}	4 V_M	6.5 I_M	26 $V_M I_M$
I_{R_4}	3 V_M	6.6 I_M	19.8 $V_M I_M$	I_{R_9}	4V_M	6.5 I_M	26 $V_M I_M$
I_{R_5}	3 V_M	6.6 I_M	19.8 $V_M I_M$	I_{R_8}	2 V_M	6.6 I_M	13.2 $V_M I_M$
I_{R_9}	3 V_M	6.6 I_M	19.8 $V_M I_M$	I_{R_3}	1 V_M	6.9 I_M	6.9 $V_M I_M$
MONOA							
I_{R_i}		$V_m(V)$		$I_R(A)$			$P(W)$
I_{R_4}		9 V_M		6.4 I_M			57.6 $V_M I_M$
I_{R_5}		9 V_M		6.4 I_M			57.6 $V_M I_M$
I_{R_6}		9 V_M		6.4 I_M			57.6 $V_M I_M$
I_{R_9}		9 V_M		6.4 I_M			57.6 $V_M I_M$
I_{R_7}		5 V_M		6.5 I_M			32.5 $V_M I_M$
I_{R_1}		4 V_M		6.6 I_M			26.4 $V_M I_M$
I_{R_2}		4 V_M		6.6 I_M			26.4 $V_M I_M$
I_{R_3}		4 V_M		6.6 I_M			26.4 $V_M I_M$
I_{R_8}		4 V_M		6.6 I_M			26.4 $V_M I_M$

Table V
Row currents and power output analysis for various reconfiguration algorithms using weighted OF for pattern 2

TCT				ASO			
I_{R_i}	$V_m(V)$	$I_R(A)$	$P(W)$	I_{R_i}	$V_m(V)$	$I_R(A)$	$P(W)$
I_{R_8}	9 V_M	6.3 I_M	56.7 V_MI_M	I_{R_2}	9 V_M	6.5 I_M	58.5 V_MI_M
I_{R_9}	9 V_M	6.3 I_M	56.7 V_MI_M	I_{R_9}	9 V_M	6.5 I_M	58.5 V_MI_M
I_{R_6}	7 V_M	6.6 I_M	46.2 V_MI_M	I_{R_8}	7 V_M	6.7 I_M	46.9 V_MI_M
I_{R_7}	7 V_M	6.6 I_M	46.2 V_MI_M	I_{R_5}	6 V_M	6.8 I_M	40.8 V_MI_M
I_{R_5}	5 V_M	7.6 I_M	38 V_MI_M	I_{R_1}	5 V_M	7.2 I_M	36 V_MI_M
I_{R_4}	5 V_M	7.6 I_M	38 V_MI_M	I_{R_7}	4 V_M	7.4 I_M	29.6 V_MI_M
I_{R_3}	5 V_M	7.6 I_M	38 V_MI_M	I_{R_3}	3 V_M	7.7 I_M	23.1 V_MI_M
I_{R_2}	2 V_M	7.8 I_M	15.6 V_MI_M	I_{R_4}	3 V_M	7.7 I_M	23.1V_MI_M
I_{R_1}	2 V_M	7.8 I_M	15.6 V_MI_M	I_{R_6}	3 V_M	7.7 I_M	23.1 V_MI_M
AVOA				IPDO			
I_{R_i}	$V_m(V)$	$I_R(A)$	$P(W)$	I_{R_i}	$V_m(V)$	$I_R(A)$	$P(W)$
I_{R_4}	9 V_M	6.9 I_M	62.1 V_MI_M	I_{R_1}	9 V_M	6.9 I_M	62.1 V_MI_M
I_{R_6}	9 V_M	6.9 I_M	62.1 V_MI_M	I_{R_4}	9 V_M	6.9 I_M	62.1 V_MI_M
I_{R_8}	9 V_M	6.9 I_M	62.1 V_MI_M	I_{R_5}	9 V_M	6.9 I_M	62.1 V_MI_M
I_{R_9}	6 V_M	7.1 I_M	42.6 V_MI_M	I_{R_7}	9 V_M	6.9 I_M	62.1 V_MI_M
I_{R_7}	5 V_M	7.2 I_M	36 V_MI_M	I_{R_9}	9 V_M	6.9 I_M	62.1 V_MI_M
I_{R_1}	7 V_M	7.3 I_M	29.2 V_MI_M	I_{R_6}	4 V_M	7.2 I_M	28.8 V_MI_M
I_{R_2}	7 V_M	7.3 I_M	29.2 V_MI_M	I_{R_8}	3 V_M	7.3 I_M	21.9 V_MI_M
I_{R_3}	7 V_M	7.3 I_M	29.2 V_MI_M	I_{R_2}	2V_M	7.6 I_M	15.2 V_MI_M
I_{R_5}	7 V_M	7.3 I_M	29.2 V_MI_M	I_{R_3}	2 V_M	7.6 I_M	15.2 V_MI_M
MONOA							
I_{R_i}		$V_m(V)$		$I_R(A)$			$P(W)$
I_{R_9}		9 V_M		6.9 I_M			62.1 V_MI_M
I_{R_6}		8 V_M		7 I_M			56 V_MI_M
I_{R_7}		8 V_M		7 I_M			56 V_MI_M
I_{R_1}		6 V_M		7.2 I_M			43.2 V_MI_M
I_{R_2}		6 V_M		7.2 I_M			43.2 V_MI_M
I_{R_3}		6 V_M		7.2 I_M			43.2 V_MI_M
I_{R_4}		6 V_M		7.2 I_M			43.2 V_MI_M
I_{R_5}		6 V_M		7.2 I_M			43.2 V_MI_M
I_{R_8}		1 V_M		7.3 I_M			7.3 V_MI_M

Table VI
Row currents and power output analysis for various reconfiguration algorithms using proposed OF for pattern 2

TCT				ASO			
I_{R_i}	$V_m(V)$	$I_R(A)$	$P(W)$	I_{R_i}	$V_m(V)$	$I_R(A)$	$P(W)$
I_{R_8}	9 V_M	6.3 I_M	56.7 V_MI_M	I_{R_1}	9 V_M	6.9 I_M	62.1 V_MI_M
I_{R_9}	9 V_M	6.3 I_M	56.7 V_MI_M	I_{R_2}	9 V_M	6.9 I_M	62.1V_MI_M
I_{R_6}	7 V_M	6.6 I_M	46.2 V_MI_M	I_{R_4}	7 V_M	7 I_M	49 V_MI_M
I_{R_7}	7 V_M	6.6 I_M	46.2 V_MI_M	I_{R_9}	6 V_M	7.1 I_M	42.6 V_MI_M
I_{R_3}	5 V_M	7.6 I_M	38 V_MI_M	I_{R_5}	5 V_M	7.2 I_M	36 V_MI_M
I_{R_4}	5 V_M	7.6I_M	38 V_MI_M	I_{R_8}	5 V_M	7.2 I_M	36 V_MI_M
I_{R_5}	5 V_M	7.6 I_M	38 V_MI_M	I_{R_3}	3 V_M	7.3 I_M	21.9 V_MI_M
I_{R_1}	2 V_M	7.6 I_M	15.6 V_MI_M	I_{R_6}	3 V_M	7.3 I_M	21.9 V_MI_M
I_{R_2}	2 V_M	7.6 I_M	15.6 V_MI_M	I_{R_7}	3 V_M	7.3 I_M	21.9 V_MI_M
AVOA				IPDO			
I_{R_i}	$V_m(V)$	$I_R(A)$	$P(W)$	I_{R_i}	$V_m(V)$	$I_R(A)$	$P(W)$
I_{R_3}	9 V_M	7 I_M	63 V_MI_M	I_{R_2}	9 V_M	7 I_M	63 V_MI_M
I_{R_4}	9 V_M	7 I_M	63 V_MI_M	I_{R_4}	9 V_M	7 I_M	63 V_MI_M
I_{R_7}	9 V_M	7 I_M	63 V_MI_M	I_{R_9}	9 V_M	7 I_M	63 V_MI_M
I_{R_1}	6 V_M	7.1 I_M	42.6 V_MI_M	I_{R_1}	6 V_M	7.2 I_M	43.2 V_MI_M
I_{R_2}	6 V_M	7.1 I_M	42.6 V_MI_M	I_{R_3}	6 V_M	7.2 I_M	43.2 V_MI_M
I_{R_6}	4 V_M	7.2 I_M	28.8 V_MI_M	I_{R_5}	6 V_M	7.2 I_M	43.2 V_MI_M
I_{R_8}	4 V_M	7.2 I_M	28.8 V_MI_M	I_{R_6}	6 V_M	7.2 I_M	43.2 V_MI_M
I_{R_5}	2 V_M	7.3 I_M	14.6 V_MI_M	I_{R_7}	6 V_M	7.2 I_M	43.2 V_MI_M
I_{R_9}	2 V_M	7.3 I_M	14.6 V_MI_M	I_{R_8}	6 V_M	7.2 I_M	43.2 V_MI_M
MONOA							
I_{R_i}		$V_m(V)$		$I_R(A)$			$P(W)$
I_{R_3}		9 V_M		7 I_M			63 V_MI_M

(*continued on next page*)

Table VI (*continued*)

MONOA			
I_{R_i}	$V_m(V)$	$I_R(A)$	$P(W)$
I_{R_4}	9 V_M	7 I_M	63 $V_M I_M$
I_{R_9}	9 V_M	7 I_M	63 $V_M I_M$
I_{R_1}	6 V_M	7.2 I_M	43.2 $V_M I_M$
I_{R_2}	6 V_M	7.2 I_M	43.2 $V_M I_M$
I_{R_5}	6 V_M	7.2 I_M	43.2 $V_M I_M$
I_{R_6}	6 V_M	7.2 I_M	43.2 $V_M I_M$
I_{R_7}	6 V_M	7.2 I_M	43.2 $V_M I_M$
I_{R_8}	6 V_M	7.2 I_M	43.2 $V_M I_M$

For seventh row,

$$I_{R7} = 4\left(\frac{900}{1000}\right)I_M + 3\left(\frac{800}{1000}\right)I_M + 1\left(\frac{400}{1000}\right)I_M + 1\left(\frac{200}{1000}\right)I_M = 6.6I_M \tag{38}$$

For eighth row,

$$I_{R8} = 5\left(\frac{900}{1000}\right)I_M + 1\left(\frac{800}{1000}\right)I_M + 1\left(\frac{600}{1000}\right)I_M + 2\left(\frac{200}{1000}\right)I_M = 6.3I_M \tag{39}$$

For the ninth row,

$$I_{R9} = 4\left(\frac{900}{1000}\right)I_M + 2\left(\frac{800}{1000}\right)I_M + 1\left(\frac{600}{1000}\right)I_M + 1\left(\frac{400}{1000}\right)I_M + 1\left(\frac{200}{1000}\right)I_M = 6.4I_M \tag{40}$$

Using the weighted OF depicted in Fig. 8 (a), MONOA algorithm evaluates row currents as follows,
For first row,

$$I_{R1} = 6\left(\frac{900}{1000}\right)I_M + 1\left(\frac{600}{1000}\right)I_M + 1\left(\frac{400}{1000}\right)I_M + 1\left(\frac{200}{1000}\right)I_M = 6.6I_M \tag{41}$$

For second row,

$$I_{R2} = 5\left(\frac{900}{1000}\right)I_M + 2\left(\frac{600}{1000}\right)I_M + 2\left(\frac{400}{1000}\right)I_M = 6.5I_M \tag{42}$$

For third row,

$$I_{R3} = 5\left(\frac{900}{1000}\right)I_M + 2\left(\frac{600}{1000}\right)I_M + 1\left(\frac{400}{1000}\right)I_M + 1\left(\frac{200}{1000}\right)I_M = 6.3I_M \tag{43}$$

For fourth row,

$$I_{R4} = 6\left(\frac{900}{1000}\right)I_M + 1\left(\frac{800}{1000}\right)I_M + 2\left(\frac{200}{1000}\right)I_M = 6.6I_M \tag{44}$$

For fifth row,

$$I_{R5} = 2\left(\frac{900}{1000}\right)I_M + 5\left(\frac{800}{1000}\right)I_M + 1\left(\frac{600}{1000}\right)I_M + 1\left(\frac{200}{1000}\right)I_M = 6.6I_M \tag{45}$$

For sixth row,

$$I_{R6} = 6\left(\frac{900}{1000}\right)I_M + 1\left(\frac{600}{1000}\right)I_M + 1\left(\frac{400}{1000}\right)I_M + 1\left(\frac{200}{1000}\right)I_M = 6.6I_M \tag{46}$$

For seventh row,

$$I_{R7} = 5\left(\frac{900}{1000}\right)I_M + 1\left(\frac{800}{1000}\right)I_M + 2\left(\frac{400}{1000}\right)I_M + 1\left(\frac{200}{1000}\right)I_M = 6.3I_M \tag{47}$$

For eighth row,

$$I_{R8} = 6\left(\frac{900}{1000}\right)I_M + 1\left(\frac{800}{1000}\right)I_M + 2\left(\frac{200}{1000}\right)I_M = 6.6I_M \tag{48}$$

For ninth row,

$$I_{R9} = 4\left(\frac{900}{1000}\right)I_M + 1\left(\frac{800}{1000}\right)I_M + 2\left(\frac{600}{1000}\right)I_M + 2\left(\frac{400}{1000}\right)I_M = 6.4I_M \tag{49}$$

Using the novel OF depicted in Fig. 8 (b), MONOA algorithm evaluates row currents as follows,
For first row,

$$I_{R1} = 4\left(\frac{900}{1000}\right)I_M + 2\left(\frac{800}{1000}\right)I_M + 2\left(\frac{600}{1000}\right)I_M + 1\left(\frac{200}{1000}\right)I_M = 6.6I_M \tag{50}$$

For second row,

$$I_{R2} = 6\left(\frac{900}{1000}\right)I_M + 1\left(\frac{600}{1000}\right)I_M + 1\left(\frac{400}{1000}\right)I_M + 1\left(\frac{200}{1000}\right)I_M = 6.6I_M \quad (51)$$

For third row,

$$I_{R3} = 6\left(\frac{900}{1000}\right)I_M + 1\left(\frac{600}{1000}\right)I_M + 1\left(\frac{400}{1000}\right)I_M + 1\left(\frac{200}{1000}\right)I_M = 6.6I_M \quad (52)$$

For fourth row,

$$I_{R4} = 4\left(\frac{900}{1000}\right)I_M + 2\left(\frac{800}{1000}\right)I_M + 1\left(\frac{600}{1000}\right)I_M + 1\left(\frac{400}{1000}\right)I_M + 1\left(\frac{200}{1000}\right)I_M = 6.4I_M \quad (53)$$

For fifth row,

$$I_{R5} = 6\left(\frac{900}{1000}\right)I_M + 2\left(\frac{400}{1000}\right)I_M + 1\left(\frac{200}{1000}\right)I_M = 6.4I_M \quad (54)$$

For sixth row,

$$I_{R6} = 4\left(\frac{900}{1000}\right)I_M + 2\left(\frac{800}{1000}\right)I_M + 1\left(\frac{600}{1000}\right)I_M + 1\left(\frac{400}{1000}\right)I_M + 1\left(\frac{200}{1000}\right)I_M = 6.4I_M \quad (55)$$

For seventh row,

$$I_{R7} = 5\left(\frac{900}{1000}\right)I_M + 1\left(\frac{800}{1000}\right)I_M + 1\left(\frac{600}{1000}\right)I_M + 1\left(\frac{400}{1000}\right)I_M + 1\left(\frac{200}{1000}\right)I_M = 6.5I_M \quad (56)$$

For eighth row,

$$I_{R8} = 6\left(\frac{900}{1000}\right)I_M + 1\left(\frac{600}{1000}\right)I_M + 1\left(\frac{400}{1000}\right)I_M + 1\left(\frac{200}{1000}\right)I_M = 6.6I_M \quad (57)$$

For ninth row,

$$I_{R9} = 4\left(\frac{900}{1000}\right)I_M + 2\left(\frac{800}{1000}\right)I_M + 1\left(\frac{600}{1000}\right)I_M + 1\left(\frac{400}{1000}\right)I_M + 1\left(\frac{200}{1000}\right)I_M = 6.4I_M \quad (58)$$

The row current values for ASO, AVOA, IPDO and MONOA are computed for pattern 1 and presented in Table 3 and Table 4, with corresponding values for pattern 2 listed in Table 5 and Table 6. Results show that algorithms using the novel OF consistently achieve higher power output across both shading patterns. For instance, PSO improves to 56.7 and 62.1 $V_M I_M$ from 55.8 to 58.5 $V_M I_M$ using the novel function. Similarly, AVOA, IPDO, and MONOA show power gains up to 57.6 and 63 $V_M I_M$. These improvements confirm that the novel OF enhances algorithm performance by guiding efficient exploration without the need for weight tuning, making it well-suited for PV array reconfiguration.

References

[1] M. Premkumar, P. Jangir, C. Ramakrishnan, G. Nalinipriya, H.H. Alhelou, B. S. Kumar, Identification of solar photovoltaic model parameters using an improved gradient-based optimization algorithm with chaotic drifts, IEEE Access 9 (2021) 62347–62379.

[2] A.R. Kalaiarasi, S. Aswin, M. Mukilan, D. Rohith, Literature review on optimizing solar panel efficiency through dynamic solar tracking, in: 2025 International Conference on Electronics and Renewable Systems (ICEARS), 2025, pp. 13–18.

[3] K.S. Kavin, P. Subha Karuvelam, M. Devesh Raj, M. Sivasubramanian, A novel KSK converter with machine learning MPPT for PV applications, Elec. Power Compon. Syst. (2024) 1–19.

[4] K.S. Kavin, P.S. Karuvelam, M. Matcha, S. Vendoti, Improved BRBFNN-based MPPT algorithm for coupled inductor KSK converter for sustainable PV system applications, Electr. Eng. (2025) 1–23.

[5] D. Yousri, T.S. Babu, E. Beshr, M.B. Eteiba, D. Allam, A robust strategy based on marine predators algorithm for large scale photovoltaic array reconfiguration to mitigate the partial shading effect on the performance of PV system, IEEE Access 8 (2020) 112407–112426.

[6] S. Rezazadeh, A. Moradzadeh, K. Pourhossein, M. Akrami, B. Mohammadi-Ivatloo, A. Anvari-Moghaddam, Photovoltaic array reconfiguration under partial shading conditions for maximum power extraction: a state-of-the-art review and new solution method, Energy Convers. Manag. 258 (2022) 115468.

[7] T.S. Babu, D. Yousri, K. Balasubramanian, Photovoltaic array reconfiguration system for maximizing the harvested power using population-based algorithms, IEEE Access 8 (2020) 109608–109624.

[8] D. Yousri, T.S. Babu, E. Beshr, M.B. Eteiba, D. Allam, A robust strategy based on marine predators algorithm for large scale photovoltaic array reconfiguration to mitigate the partial shading effect on the performance of PV system, IEEE Access 8 (2020) 112407–112426.

[9] M. Alkahtani, Z. Wu, C.S. Kuka, M.S. Alahammad, K. Ni, A Novel PV array reconfiguration algorithm approach to optimising power generation across non-uniformly aged PV arrays by merely repositioning, Op J. 3 (1) (2020) 5.

[10] C.V. Chandrakant, S. Mikkili, A typical review on static reconfiguration strategies in photovoltaic array under non-uniform shading conditions, CSEE J. Power Energy Syst. 9 (6) (2020) 2018–2039.

[11] M.N. Nazeri, M.F. Tajuddin, T.S. Babu, A. Azmi, M. Malvoni, N.M. Kumar, Firefly algorithm-based photovoltaic array reconfiguration for maximum power extraction during mismatch conditions, Sustainability 13 (6) (2021) 3206.

[12] B. Yang, R. Shao, M. Zhang, H. Ye, B. Liu, T. Bao, J. Wang, H. Shu, Y. Ren, H. Ye, Socio-inspired democratic political algorithm for optimal PV array reconfiguration to mitigate partial shading, Sustain. Energy Technol. Assessments 48 (2021) 101627.

[13] G.H. Varma, V.R. Barry, R.K. Jain, D. Kumar, An MMTES algorithm for dynamic photovoltaic array reconfiguration to enhance power output under partial shading conditions, IET Renew. Power Gener. 15 (4) (2021) 809–820.

[14] S. Rezazadeh, A. Moradzadeh, S.M. Hashemzadeh, K. Pourhossein, B. Mohammadi-Ivatloo, S.H. Hosseini, A novel prime numbers-based PV array reconfiguration solution to produce maximum energy under partial shade conditions, Sustain. Energy Technol. Assessments 47 (2021) 101498.

[15] V.M. Tatabhatla, A. Agarwal, T. Kanumuri, A chaos map based reconfiguration of solar array to mitigate the effects of partial shading, IEEE Trans. Energy Convers. 37 (2) (2021) 811–823.

[16] D. Yousri, S.B. Thanikanti, K. Balasubramanian, A. Osama, Multi-objective grey wolf optimizer for optimal design of switching matrix for shaded PV array dynamic reconfiguration, IEEE Access 8 (2020) 159931–159946.

[17] H. Rezk, A. Fathy, M. Aly, A robust photovoltaic array reconfiguration strategy based on coyote optimization algorithm for enhancing the extracted power under partial shadow condition, Energy Rep. 7 (2021) 109–124.

[18] N.K. Solaisamy, P.W. David, P. Murugesan, Performance improvement of partial shaded solar PV system using Unbalanced adaptive dynamic reconfiguration technique, Renew. Energy 246 (2025) 122883.

[19] A. Loukriz, M. Kichene, A. Bendib, M. Drif, D. Saigaa, H. Ahmed, Improved dynamic reconfiguration strategy for power maximization of TCT interconnected PV arrays under partial shading conditions, Electr. Eng. 107 (1) (2025) 459–470.

[20] N.A. Kadhim, A.A. Obed, A.J. Abid, A.L. Saleh, R.J. Hassoon, A systematic review for reconfiguring photovoltaic arrays under conditions of partial shading, Electr. Eng. Techn. J. 1 (1) (2024) 20–34.

[21] N.A. Kadhim, A.A. Obed, A.J. Abid, H. Kotb, A. Emara, Optimal PV reconfiguration under partial shading based on white shark optimization, IEEE Access 12 (2024) 27385–27398.
[22] I.U. Khalil, M. Jalal, A. ul Haq, M. Ahsan, U. Ghumman, A fuzzy reconfiguration approach for mitigating power losses in PV systems, Results Eng. 25 (2025) 103965.
[23] H.I. Solis-Cisneros, P.Y. Sevilla-Camacho, J.B. Robles-Ocampo, M.A. Zuñiga-Reyes, J. Rodríguez-Resendíz, J. Muñiz-Soria, C.A. Hernández-Gutiérrez, A dynamic reconfiguration method based on neuro-fuzzy control algorithm for partially shaded PV arrays, Sustain. Energy Technol. Assessm. 52 (2022) 102147.
[24] S. Li, T. Zhang, J. Yu, Photovoltaic array dynamic reconfiguration based on an improved pelican optimization algorithm, Electronics 12 (15) (2023) 3317.
[25] X. Zhang, D. Meng, W. Li, T. Yu, Z. Fan, Z. Hao, Evolutionary based pareto optimization algorithms for bi-objective PV array reconfiguration under partial shading conditions, Energy Convers. Manag. 271 (2022) 116308.
[26] S.K. Shakthivel, P.W. David, S. Periya Backiyam, M.S. Murugan, Square dynamic reconfiguration for the partial shaded photovoltaic system–simulation and experimental analysis, Energy Sources, Part A Recovery, Util. Environ. Eff. 44 (3) (2022) 6868–6885.
[27] M. Durango-Flórez, D. González-Montoya, L.A. Trejos-Grisales, C.A. Ramos-Paja, PV array reconfiguration based on genetic algorithm for maximum power extraction and energy impact analysis, Sustainability 14 (7) (2022) 3764.
[28] C. Janani, B. Chitti Babu, K. Vijayakumar, An optimized reconfiguration technique of photovoltaic array using adaptive-JAYA optimization, Energy Sources, Part A Recovery, Util. Environ. Eff. 45 (2) (2023) 3777–3810.
[29] B. Yang, Y. Hu, H. Ye, J. Zhang, X. Cheng, Z. Li, Y. Ren, Y. Yan, Design and HIL validation of improved prairie dog optimization based dynamic unitary reconfiguration for partially shaded PV arrays, Sol. Energy 269 (2024) 112361.
[30] D. Li, H. Zhou, Y. Zhou, Y. Rao, W. Yao, Atom search optimization-based PV array reconfiguration technique under partial shading condition, Int. Transact. Electr. Energ. Syst. 2023 (1) (2023) 8685976.
[31] M. Alanazi, A. Fathy, D. Yousri, H. Rezk, Optimal reconfiguration of shaded PV based system using African vultures optimization approach, Alex. Eng. J. 61 (12) (2022) 12159–12185.